THE PUBLISHING HOUSE
OF THE ROMANIAN ACADEMY

PROCEEDINGS OF THE ROMANIAN ACADEMY, Series A,
Volume 22, Number 2/2021, pp. 163–170

ON THE HUMAN LIVER DEFORMATION DURING ROBOTIC NEEDLE INSERTION

Veturia CHIROIU, Nicoleta NEDELCU, Ligia MUNTEANU, Cristian RUGINĂ, Marius IONESCU, Ciprian DRAGNE

Institute of Solid Mechanics of the Romanian Academy – Ctin Mille 15, 010141 Bucharest, Romania

Corresponding author: Veturia CHIROIU, E-mail: veturia.chiroiu@imsar.ro

Abstract. This paper formulates and motivates a model for deformation of the surgical needle during its insertion into the human liver. The motion equations of the needle are similar to Tzitzeica equations of surfaces which are invariant under the group of centro-affine transformations. That means the surfaces tend to minimize their area and have a minimal Dirichlet energy of how variable a function is. The closed form solutions are obtained for deformation of the needle. In addition, the collision between the needle and the tissues is modeled as a minimization problem.

***Key words**:* surgical needle, human liver, deformation, collision.

1. INTRODUCTION

Estimation the surgical needle deformation during the insertion into the human liver can be expressed as a problem of optimization of the cutting procedures for malignant hepatic tumors [1–3]. The optimization includes the minimization of the damage to the patient body by choosing flexible, long and slender surgical needle in order to cause minimum needle deflections during insertion procedures [4–7].

The treatment of non-respectable hepatic tumors is obtained by transporting into the tumor of an active chemical agent with the help of a surgical needle. The trajectories of the needle must not collide with other organs or tissues, blood vessels or nerves. In this paper, the Lagrangian formulation is used to model the flexible needle as a Euler-Bernoulli beam within the framework of the linear elasticity theory. Fig. 1 presents the tumor position and possible collision-free trajectories of the surgical needle.

Consider a serial surgical robot consisting of two revolute joints, a flexible arm and a flexible needle. The configuration of the elastic beam is described by the position and orientation of the frame $K_1(x_1, y_1)$, and the configuration of the needle is described in the frame $K_2(x_2, y_2)$ (Fig. 2). The position and orientation of K_1 and K_2 is given by the shape matrix. The robot has *f* degrees of freedom $f = f_r + f_e$, $f_e = \sum_{i=1}^{2} f_{ei}$, where $f_r = 2$ are the rigid body degrees of freedom, and $f_e = 2$ are the elastic degrees of freedom resulting from the 2D bending of the flexible arm and the needle [8–11].

In this paper a surgical robot consisted of a revolute joint and a flexible needle is considered (Fig. 1). The Lagrange reference system of coordinates (X, Y, Z) of unit vectors $(\mathbf{e}_1, \mathbf{e}_2, \mathbf{e}_3)$ with the origin *O* located in the entry point of the skin is attached to the needle. A local Euler system of coordinate with the unit vectors $(\mathbf{d}_1, \mathbf{d}_2, \mathbf{d}_3)$ is attached to the flexible needle to describe the position and orientation of the needle who must carry drugs to the tumor. The angle between the needle and the axis x_1 is $\tilde{\theta}_1$, which represents the generalized coordinate of the rigid system. The serial robot has *f* degrees of freedom $f = f_r + f_e$, where $f_r = 1$ is the rigid body degree of freedom, and $f_e = 3$ are the elastic degrees of freedom representing the deformations of the needle at bending u_1, u_2 and torsion u_3. The generalized coordinates vector is $\mathbf{q} = \left[\tilde{\theta}_1, u_1, u_2, u_3\right]^{\mathrm{T}}$.

The environment containing the organs, ribs, blood vessels and the tumor and possible collision-free trajectories of the surgical needle are represented in Fig. 2.

Different types of needles were analyzed before choosing the surgical needle [12–14]. The flexible bee barbed needle proposed by Sahlabadi [14] is chosen for some of its advantages such as: it decreases the most the insertion force, that is with 24%, and therefore it decreases the tissue deformation by 17% because of the tip deflection. The characteristics of this needle are: the front angle has 157 deg, the back angle, 110 deg, the height is 0.5 mm, and the tip thickness 0.15 mm. The honeybee barbed needle model is presented in Fig. 3 [9, 15, 16].

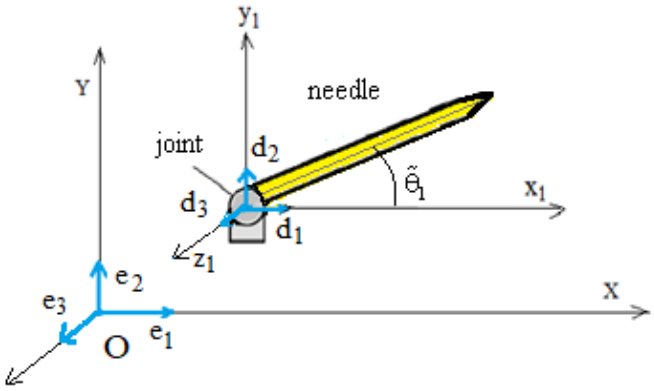

Fig.1 – Surgical robot consisted of a revolute joint and a flexible needle.
The Lagrange coordinate system OXY and the local Euler coordinate systems are attached to flexible needle.

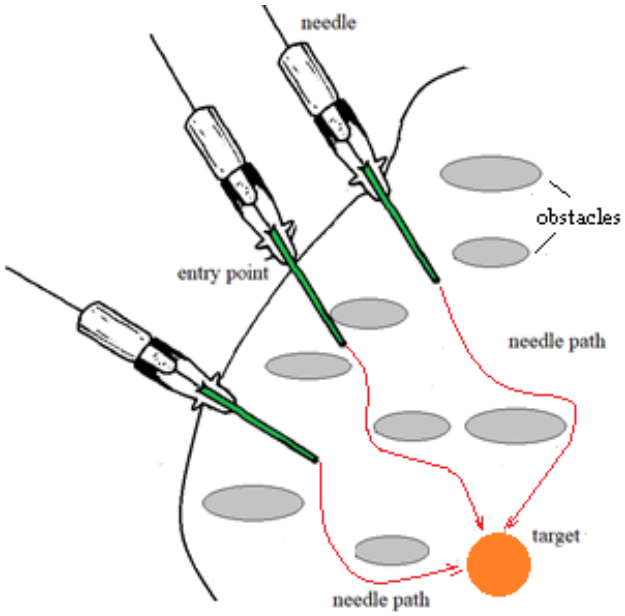

Fig. 2 – Tumor position and possible collision-free trajectories of the surgical needle.

2. MODELING THE FLEXIBLE NEEDLE INSERTION INTO THE HUMAN LIVER

The flexible needle is modeled as an elastic thread within the framework of the elastic theory of the thin elastic thread [17, 18]. The limitation of the current methods existing in the literature consists in applying only 1D linear elasticity theories to a 3D problem with significant nonlinear properties [19].

In what follows, we present some results which fill a gap in the simulation of the surgical needle deformation because, despite the current methods in the modeling of the needle response during its insertion into the tumor, no realistic methods and results have been identified.

Let us consider the case of a tumor located in a difficult place to be reached in the vicinity of the portal tree in the vascular territory of the liver. Location of the tumor, the vascular territory and the vessel branches in the vicinity of the tumor are displayed in Fig. 4.

Figure 4a represents the location of the tumor and Fig. 4b the vascular territory and the vessel branches in the vicinity of the tumor. It is assumed that the collision-free needle trajectory towards the tumor can take any form even if physically they cannot be realized.

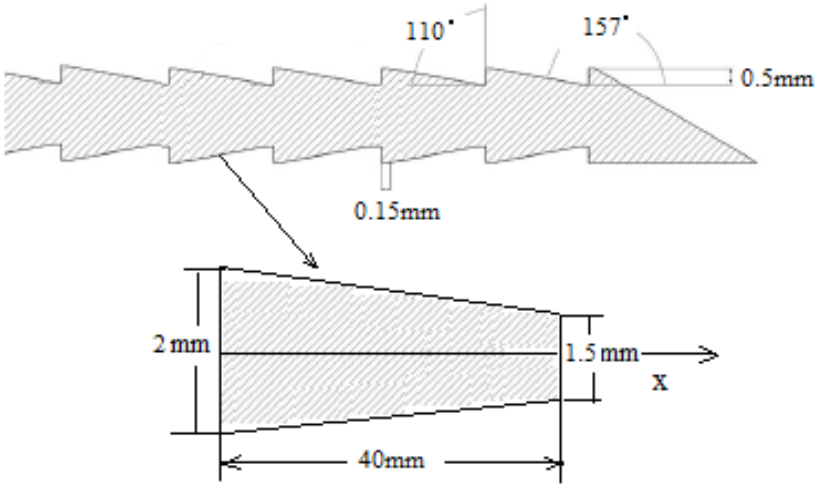

Fig. 3 – Honeybee barbed needle model inspired from [13].

The medical robot is designed for interventions that are difficult to perform in the classic way. In this sense, the restrictions refer to the minimal destruction of healthy tissues (no wrong cuts, no sectioning of blood vessels or nerves). The simplest and most natural shape of the needle trajectory is the straight line which connects the point of entry into the skin to the tumor. But in the most cases, the trajectory can take different forms due to the restriction of avoiding collisions with organs and tissues. Possible such trajectories are displayed in Fig. 5, but the optimal shape of the trajectories is obtained from an optimization problem.

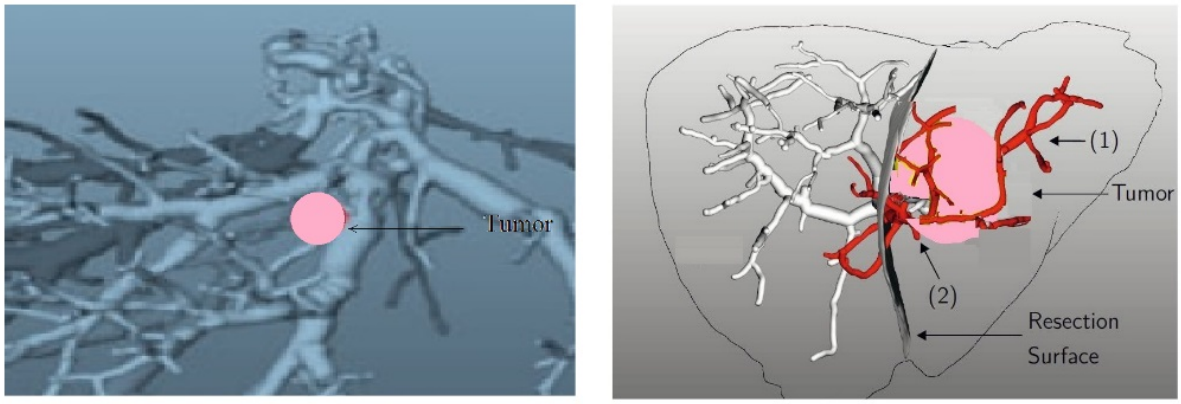

Fig. 4 – a) Location of the tumor; b) vascular territory (1) and the vessel branches in the vicinity of tumor (2).

The optimization problem of determining the free-collision trajectories of the surgical needle must take into account all difficulties which occur in such operation: (1) the needle must solve its task of transporting drugs into the tumor, (2) the insertion trajectory of the needle should avoid the ribs, blood vessels, and other tissues and organs in the abdominal cavity.

The minimum distance problem can be modeled as a minimization problem that checks the minimum distance between the needle and the tissue [7, 19]

$$\min\left(\frac{1}{2}(\mathbf{r}_1-\mathbf{r}_2)^{\mathrm{T}}(\mathbf{r}_1-\mathbf{r}_2)\right), \tag{1}$$

with $\mathbf{r}_1, \mathbf{r}_2$ the position vectors of two points belonging to the needle and the tissue. The interference distance or penetration is expressed as

$$\min(-d), \quad g_1(\mathbf{r}_1) \le -\frac{d}{2}, \quad g_2(\mathbf{r}_2) \le -\frac{d}{2}, \tag{2}$$

where d is the penetration and g_1, g_2 are the surfaces to the needle and the tissue, respectively.

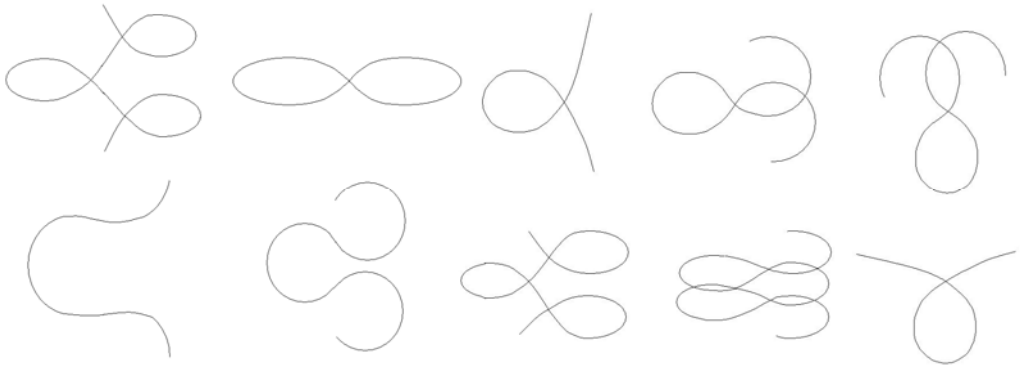

Fig. 5 – Different shapes for a trajectory.

Let s be the coordinate along the central line of the natural state of the needle. The simulation is performed for a bee needle made from shape memory alloys with 55% Nickel and 45% titanium, with density $\rho = 6.5$ kg/m^3, the modulus of elasticity $E = 32.3$ GPa at bending, and the Poisson's ratio $\nu = 0.48$.

The Lagrange technique is used to obtain the motion equations of the needle with the ends fixed by the force $\mathbf{F} = -\mathbf{f}$ with $\mathbf{f} = (f_1, f_2, f_3)$. This force describes the contact between the needle and the tissue $\mathbf{f} = p_c \mathbf{n}$. The prime means the partial differentiation with respect to s. The motion equations of the surgical needle are obtained as [7, 17]

$$-\rho \ddot{\mathbf{r}} - \mathbf{f}' = 0 \tag{3}$$

$$\begin{aligned} k_1(\dot{\psi}^2 \sin\theta\cos\theta - \ddot{\theta}) - k_2(\dot{\varphi} + \dot{\psi}\cos\theta)\dot{\psi}\sin\theta - A(\psi'^2 \sin\theta\cos\theta - \theta'') + C(\varphi' + \psi'\cos\theta)\psi'\sin\theta - \\ - f_1\cos\theta\cos\psi - f_2\cos\theta\sin\psi + f_3\sin\theta = 0, \end{aligned} \tag{4}$$

$$\begin{aligned} -\frac{\partial}{\partial t}\left\{k_1\dot{\psi}\sin^2\theta + k_2(\dot{\varphi} + \dot{\psi}\cos\theta)\cos\theta\right\} + \frac{\partial}{\partial s}\left\{A\psi'^2\sin^2\theta + C(\varphi' + \psi'\cos\theta)\cos\theta\right\} + \\ + f_1\sin\theta\sin\psi - f_2\sin\theta\cos\psi = 0, \end{aligned} \tag{5}$$

$$-k_2\frac{\partial}{\partial t}(\dot{\varphi} + \dot{\psi}\cos\theta) + C\frac{\partial}{\partial s}(\varphi' + \psi'\cos\theta) = 0. \tag{6}$$

where θ, ψ and φ are the Euler angles, $r(s,t)$ is the position vector which can be interpreted as the image of the central axis in the Euler configuration, $f = (f_1, f_2, f_3)$ is the force applied to the needle, ρ is the mass density per unit volume, A and C are the bending stiffness and respectively the torsional stiffness of the needle, related to the Lamé constants λ, μ by $A = \frac{1}{4}\pi a^4 E$, $C = \frac{1}{2}\pi a^4 \mu$, where E is the flexural Young's modulus, and a is the radius of the cross section of the needle. The dot means the differentiation with respect to time.

The unknowns in the motion equations (3–6) are the Euler angles θ, ψ and φ. The system of equations (3–6) are solved by the cnoidal method [17]. The method is reducible to a generalization of the Fourier series with the cnoidal functions as the fundamental basis function. This is because the cnoidal functions are much richer than the trigonometric or hyperbolic functions, that is, the modulus m of the cnoidal function, $0 \le m \le 1$, can be varied to obtain a sine or cosine function $(m \cong 0)$, a Stokes function $(m \cong 0.5)$ or a solitonic function, sech or tanh $(m \cong 1)$.

The relationship between the Euler angles and the needle deformation is given by

$$\begin{aligned} u_1 &= \theta' \sin\varphi - \psi' \sin\theta \cos\varphi, \\ u_2 &= \theta' \cos\varphi + \psi' \sin\theta \sin\varphi, \\ u_3 &= \varphi' + \psi' \cos\theta \ . \end{aligned} \tag{7}$$

The functions (u_1, u_2, u_3) measure the bending and torsion of the needle.

3. RESULTS

The minimization problem (1, 2) is solved by using a genetic algorithm [18]. The objective function is minimized

$$\Im = \sum_{i=1}^{N} \left[\left(\frac{1}{2} (\mathbf{r}_{1i} - \mathbf{r}_{2i})^{\mathrm{T}} (\mathbf{r}_{1i} - \mathbf{r}_{2i}) \right) \right]^2, \tag{8}$$

subjected to restrictions

$$\min(-d), \quad \mathrm{g}_1(\mathbf{r}_1) \le -\frac{d}{2}, \quad \mathrm{g}_2(\mathbf{r}_2) \le -\frac{d}{2}. \tag{9}$$

Three locally 2D optimal collision-free trajectories for the surgical needle corresponding to three different entry points into the skin A, B and C are displayed in Fig. 6 [11].

The motion equations (3–6) possess a special type of solutions. These solutions known as *solitons* are localized functions that conserve their properties even after interaction among them, and then act somewhat like particles [17]. In addition, these equations are invariants under the group of centro-affine transformations, being similar to the partial differential equations which arise in the Tzitzeica surfaces theory [19]. Tzitzeica surfaces that have the essential property to be invariant under the group of centro-affine transformations [17, 19]. That means that the surfaces locally tend to minimize their area and to have a minimal Dirichlet energy that measures of how variable a function is. With other words, the surfaces have only local optima, not global optima and the functions are stable with no tendency towards the chaos.

The closed form solutions of the Euler angles θ, ψ and φ are given by [17]

$$\begin{aligned} \cos\theta = \zeta &= \zeta_2 - (\zeta_2 - \zeta_3)\,\mathrm{cn}^2\left(\sqrt{\frac{|f_3|}{2A}(\zeta_1 - \zeta_3)}(\xi - \xi_3), m\right) = \\ &= \zeta_2 - (\zeta_2 - \zeta_3)\,\mathrm{cn}^2\left[w(\xi - \xi_3), m\right], \end{aligned} \tag{10}$$

$$\begin{aligned} \psi = \frac{1}{4(A - k_1 v^2)^2 w^2} \Bigg\{ & -\frac{\beta + (C - k_2 v^2)\tau}{1 - \zeta_3} \Pi\left[w(\xi - \xi_3), \frac{\zeta_2 - \zeta_3}{1 - u_3}, m \right] - \\ & -\frac{\beta - (C - k_2 v^2)\tau}{1 + \zeta u_3} \Pi\left[w(\xi - \xi_3), \frac{\zeta_2 - \zeta_3}{1 + u_3}, m \right] \Bigg\}, \end{aligned} \tag{11}$$

$$\varphi=-\frac{\tau\left[C-A-(k_2+k_1)v^2\right]}{A-k_1v^2}\xi+\frac{1}{4(A-k_1v^2)^2w^2}\left\{\frac{\beta+(C-k_2v^2)\tau}{1-\zeta_3}\Pi\left[w(\xi-\xi_3),\frac{\zeta_2-\zeta_3}{1-\zeta_3},m\right]-\right.$$
$$\left.-\frac{\beta-(C-k_2v^2)\tau}{1+\zeta_3}\Pi\left[w(\xi-\xi_3),\frac{\zeta_2-\zeta_3}{1+\zeta_3},m\right]\right\}, \tag{12}$$

where $m=\frac{\zeta_2-\zeta_3}{\zeta_1-\zeta_3}$ and $w=\sqrt{\frac{|f_3|}{2A}(\zeta_1-\zeta_3)}$, $\Pi(x,z,m)=\int_0^x\frac{\mathrm{d}y}{1-z\,\mathrm{sn}^2(y,m)}$ is the normal elliptic integral of the third kind. Functions ζ_1,ζ_2,ζ_3 are solutions of the Weierstrass equation

$$\frac{1}{2}\zeta'^2=a\zeta^3+b\zeta^2-a\zeta+c, \tag{13}$$

$$a=-\frac{f_3}{A}\neq 0,\quad b=\frac{1}{2A}\left(\gamma-\frac{C^2\tau^2}{A}\right),\quad c=-\frac{1}{2A}\left(\gamma-\frac{\beta^2}{A}\right),$$

which admits the soliton solutions [17].

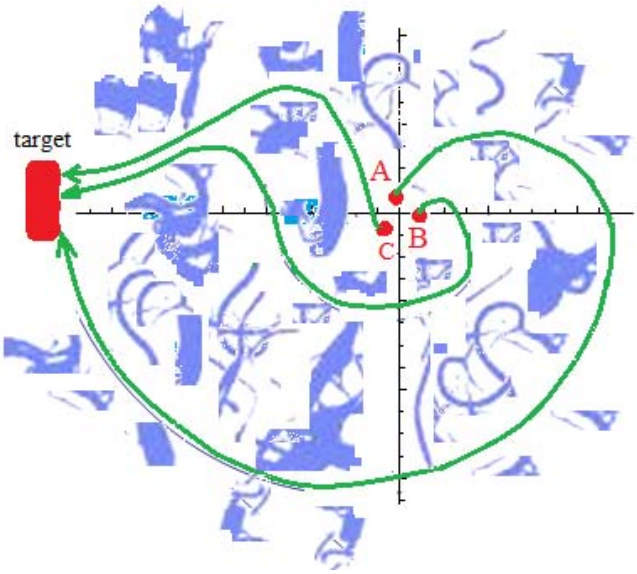

Fig. 6 – Three 2D optimal collision-free trajectories for the needle robot.

The deformation of the needle during navigation into the liver towards the tumor is represented in Fig. 7. The bending deformation u_1 and u_2 are shown in Fig. 7a and the torsion deformation u_3 of the needle in Fig. 7b, respectively. While the deformation of the surgical needle has been extensively studied [9, 15–18] many features of the needle behavior remain to be investigated.

Important characteristics of the needle deformation are obtained by intersection of the surfaces u_1,u_2,u_3 with $z=\text{const}$. The 2D hyperbolic manifolds (x,y) with the curvature const/a^4 are obtained. We recognize here the Tzitzeica surfaces which have only local optima not global optima [13]. That means that the deformation of the needle has periodicity properties. The mechanical properties of the human liver are investigated in [9, 15–19] by using a basic functional unit of the liver which comprises a hexagonal and a portal triad -portal vein, hepatic artery, bile duct. The sonification technique for hardly detectable details in the medical images is also applied for the microscopic investigation of the human liver [15]. The 3D manifold of the Tzitzeica variety includes a solid torus and three thickened deformation surfaces, as shown in Fig. 8. Details on this issue can be found in [20–27].

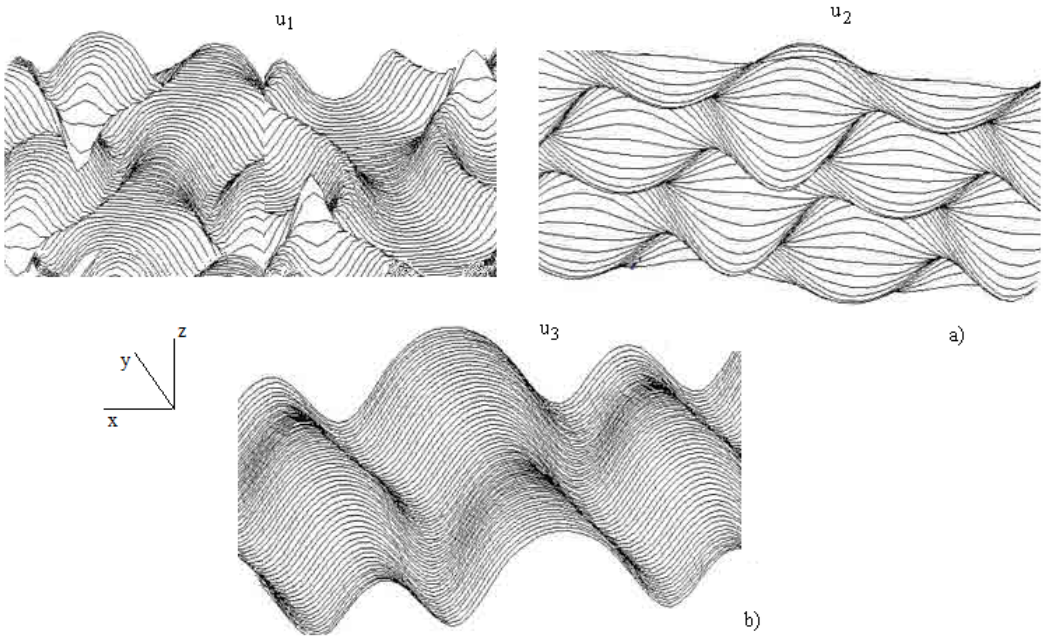

Fig. 7 – a) The bending deformation u_1 and u_2 ; b) the torsion deformation u_3 of the needle.

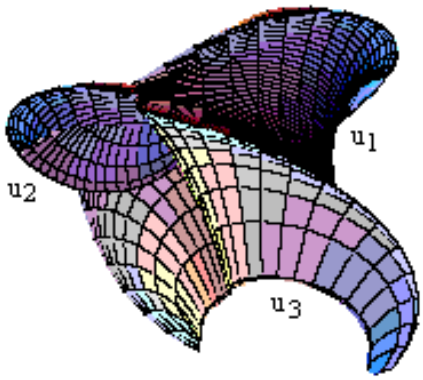

Fig. 8 – The 3D manifold of a Tzitzeica surface.

4. CONCLUSIONS

The surgical bee needle deformation during the insertion into the human liver is considered difficult because of the complexity and variability of the liver. Based on the thin elastic thread theory, the deformation of the bee needle during insertion into the human liver is analyzed.

The motion equations of the needle are similar to equations which arise in the Tzitzeica surfaces and therefore, these equations reveal their invariant properties under the group of centro-affine transformations.

This trend is to minimize the surface area and the Dirichlet energy that measures the stability of the needle deformations. The closed form solutions are obtained for bending and torsion of the needle. The modeling of the collision between the needle and the tissues as a minimization problem that checks the minimum distance between the needle and the tissue is also developed.

ACKNOWLEDGMENTS

This work was supported by a grant of the Romanian Ministry of Research and Innovation, project number PN-III-P1-1.2-PCCDI-2017-0221/ 59 PCCDI/2018 (IMPROVE). Each author has contributed equally for the paper.

REFERENCES

1. D. GAO, Y. LEI, B. LIAN, B.YAO, *Modeling and simulation of flexible needle insertion into soft tissue using modified local constraints*, Journal of Manufacturing Science and Engineering, **138**, p. 121012, 2016.
2. D. PISLA, C., VAIDA, I. BIRLESCU, B., GHERMAN, N. PLITEA, N., *Risk management for the reliability of robotic assisted treatment of non-resectable liver tumors*, Applied sciences, **10**, *9*, p. 52, 2020.
3. S.P. DiMAIO, S.E. SALCUDEAN, *Needle insertion modeling and simulation*, IEEE Trans. Robot. Automat., **19**, pp. 864–875, 2003.
4. R. ALTEROVITZ, K. GOLDBERG, A. OKAMURA, *Planning for steerable bevel-tip needle insertion through 2d soft tissue with obstacles*, Proc. of ICRA, pp. 1640–1645, 2005.
5. S.E. SALCUDEAN, D. FRENCH, S. BACHMANN, R. ZAHIRI-AZAR, *Viscoelasticity modeling of the prostate region using vibro-elastography*, Proc. of MICCAI, pp. 389–396, 2006.
6. C. VAIDA, N. PLITEA, N. AL HAJJAR, A. BURZ, F. GRAUR, B. GHERMAN, D. PISLA, *A new robotic system for minimally invasive treatment of liver tumours*, Proceedings of the Romanian Academy, Series A, **21**, *3*, pp. 263–271, 2020.
7. V. CHIROIU, L. MUNTEANU, C. RUGINĂ, N. Nedelcu, *Modeling of the flexible needle insertion into the human liver*, Chap. 2, In: *Biomedical signal and image processing* (Ed. Y. Zhou), pp. 25–40, IntechOpen, London, 2021.
8. L. MUNTEANU, C. RUGINA, C. DRAGNE, V. CHIROIU, *On the robotic control based on interactive activities of subjects*, Proceedings of the Romanian Academy, Series A, **21**, *2*, pp. 173–178, 2020.
9. V. CHIROIU, L. MUNTEANU, R. IOAN, C. DRAGNE, L. MAJERCSIK, *Using the sonification for hardly detectable details in medical images*, Scientific Reports, **9**, p. 17711, 2019.
10. F. GIULIANTE, F. AEDITO, M. VELLONE, G. NUZZO, *Segment 4b: Laparoscopic approach*, chap. 30, In: *Minimally invasive surgery of the liver* (Eds. F. Calise, L. Casciola), pp. 213–217, Springer, 2013.
11. C. DRAGNE, V. CHIROIU, L. MUNTEANU, C. BRIȘAN, C. RUGINĂ, R. IOAN, N.-D. STĂNESCU, A. STAN, *On the collision free-trajectories of a multiple-needle robot based on the Fibonacci sequence*, EuCoMeS 2020: New Trends in Mechanism and Machine Science, pp. 169–180, Mechanisms and Machine Science Series, Vol. 89, Springer, 2019.
12. M.H. KORAYEM, A. NIKOOBIN, V. AZIMIRAD, *Trajectory optimization of flexible link manipulators in point-to point motion*, Robotica, **27**, pp. 825–840, 2009.
13. M. HILLER, M. SCHNEIDER, *Modelling, simulation and control of flexible manipulators*, Eur. J. Mech., A/Solids, **16**, pp. 127–150, 1997.
14. M. SAHLABADI, P. HUTAPEA, *Tissue deformation and insertion force of bee-stinger inspired surgical needles*, Journal of Medical Devices, **12**, p. 034501, 2018.
15. V. CHIROIU, N. NEDELCU, D. PISLA, L. MUNTEANU, C. RUGINĂ, *On the mechanical properties of the human liver*, Scientific Reports, **11**, p. 10251, 2021.
16. V. CHIROIU, C. BRIȘAN, L. MUNTEANU, C. RUGINĂ, *On self-motions of planar Stewart-Gough platforms*, International Journal of Architectural Engineering Technology, **8**, p. 14–21, 2021.
17. L. MUNTEANU, St. DONESCU, *Introduction to soliton theory: applications to mechanics*, Book Series Fundamental Theories of Physics, Vol. 143, Kluwer Academic Publishers, Dordrecht, Boston (Springer Netherlands), 2004.
18. C. BRI□AN, C. BOANTĂ, V. CHIROIU, *Introduction in optimization of industrial robots: theory and applications*, Editura Academiei Române, Bucharest, 2019.
19. G. TZITZEICA, *Géométrie projective différentielle des réseaux*, Editura Cultura Națională, Bucarest and Gauthier-Villars, Paris, 1924.
20. B. KERBL, *Intervention planning of hepatocellular carcinoma radio-frequency ablations*, Clinical Image-Based Procedures from Planning to Intervention International Workshop (CLIP2012), France, In: *Notes in Computer Science*, **7761**, pp. 9–16, Springer, 2013.
21. M. CIAVARELLA, *Generalized Cattaneo partial slip plane contact problem I-Theory*, International Journal of Solids and Structures, **35**, *18*, pp. 2349–4362, 1998.
22. M. CIAVARELLA, *Generalized Cattaneo partial slip plane contact problem II-Examples*, International Journal of Solids and Structures, **35**, *18*, pp. 2363–2378,1998.
23. J. JAEGER, *Analytical solutions of contact impact problems*, Applied Mechanics Reviews, **47**, *2*, pp. 35–54, 1994.
24. M. HILLER, M. KECSKEMETHY, *Dynamics of multibody systems with minimal coordinates*, Proceedings of the NATO-Advances Study Institute on Computer Aided Analysis of Rigid and Flexible Mechanical Systems (Eds. M.S. Pereira, J.A.C. Ambrosio), Vol. 1, pp. 119–163, Troia, Portugal, Kluwer Academic Publishers, 1993.
25. M. HILLER, C. WOERNLE, *The characteristic pair of joints-an effective approach for the solution of the inverse kinematics problem for robots*, Proceedings of the International Conference on Robotics and Automation, pp. 846–851, Philadelphia, IEEE, 1988.
26. B.C. BOUSGARROU, P. RAY, G. GOGU, *New approach for dynamic modeling of flexible manipulators*, Proc. IMechE Part K: J. Multi-body Dynamics, **219**, pp. 285-298, 2003.
27. J.D. LEE, *Optimal control of a flexible parallel link robotic manipulator*, Computers and Structures, **48**, *3*, pp. 375–385, 1993.

Received August 6, 2020